Available online at www.sciencedirect.com
ScienceDirect
Trans. Nonferrous Met. Soc. China 33(2023) 1665−1676
Transactions of Nonferrous Metals Society of China
www.tnmsc.cn

# Effects of welding layer arrangement on microstructure and mechanical properties of gas metal arc welded 5083/6005A aluminium alloy butt joints

Lai-jun WU[1,2], Xiao-hui HAN[3], Guo-long MA[3], Biao YANG[1,2], Hong BIAN[1,2], Xiao-guo SONG[1,2], Cai-wang TAN[1,2]

1. State Key Laboratory of Advanced Welding and Joining, Harbin Institute of Technology, Harbin 150001, China;
2. Shandong Provincial Key Laboratory of Special Welding Technology, Harbin Institute of Technology at Weihai, Weihai 264209, China;
3. CRRC Qingdao Sifang Co., Ltd., Qingdao 266111, China

Received 30 December 2021; accepted 26 April 2022

**Abstract:** The effects of welding layer arrangement on the microstructure and mechanical properties of 5083/6005A aluminium alloy gas metal arc welded (GMAW) joints were studied. High-quality butt joints were obtained under different welding layer arrangements, including two layers and two passes, two layers and three passes, and three layers and three passes. The results indicated that the softening zone located in the heat-affected zone (HAZ) of the 6005A aluminium alloy side was the weakest part of the 5083/6005A alloy joints. The highest level of recrystallization and precipitate dissolution was observed in the HAZ of the two-layer and two-pass joints; however, the lowest level was verified in the three-layer and three-pass joints. With the increase in the number of welding layers and passes, grain boundary liquation in the partially melted zone (PMZ) and strength loss of the softened zone were improved. The tensile strength of the two-layer and two-pass joints was 161 MPa, while that of the three-layer and three-pass joints increased to 217 MPa.

**Key words:** aluminium alloy; gas metal arc welding; welding layer arrangement; microstructure; mechanical properties

## 1 Introduction

Recently, aluminium alloy applications have been a hot spot for transportation in the field of high-speed train manufacturing to obtain a low-mass structure and reduce the energy consumption [1−3]. For example, the 5xxx and 6xxx series aluminium alloys are widely used in assembling the body frame of the new generations of China Railway High-speed (CRH) trains. A lighter body frame will contribute to a further increase in the train running speed [4].

The 5xxx Al alloy belongs to the Al−Mg-based alloys, which are not heat-treatable and mainly reinforced by Mg element solution strengthening and cold-work hardening effects [5]. The 5xxx Al alloy fusion-welded joints are slightly affected by welding thermal cycles, and the tensile strength can reach 90% of the base metal according to recent studies [6,7]. The 6xxx Al alloy is an age-hardening aluminium alloy. Its main alloying elements Mg and Si formed a strengthening precipitate $\beta''$ phase [8]. The 6xxx Al alloy possesses excellent plasticity and formability. Unfortunately, the mechanical performance of the 6xxx Al alloy is easily affected by the welding thermal cycles. The high peak temperature in the weld regions will dissolve the $\beta''$ phase and the rapid cooling restricts reprecipitation, leading to severe softening in the heat-affected zone (HAZ) [9]. Moreover, dynamic recrystallization in the HAZ generally further induces strength loss. LIU et al [10] found that the microhardness of 6005A CMT welds declined to HV 50 in the HAZ

**Corresponding author:** Cai-wang TAN, Tel: +86-15065120769, E-mail: tancaiwang@hitwh.edu.cn
DOI: 10.1016/S1003-6326(23)66212-0

while reaching HV 90 in the base metal owing to the dissolution of $\beta''$ precipitates and an enlarged grain size. LIU et al [11] demonstrated that the softening HAZ became the weakest region in 6005A welds and the ultimate tensile strength only reached 70% of the base metal.

The joints of dissimilar aluminium alloys have received extensive attention because it is considered as a good strategy to develop light-weight hybrid component. YAN et al [12] joined 6xxx and 7xxx Al alloys by friction stir welding and reported that the joints failed on the HAZ of 6xxx Al alloy side in tensile tests. GUNGOR et al [13] reported that high heat input of MIG welding was the key factor to cause the softening, and they successfully welded 5083 and 6082 Al alloys by adopting cold metal transfer (CMT) welding with much low heat input.

Multilayer and multipass gas metal arc welding (GMAW) of 5083/6005A dissimilar aluminium alloys is very common in manufacturing the body frame of CRH trains. In the multilayer and multipass welding of aluminium alloys, the welded joints experience different welding thermal cycles under different welding layer arrangements, so the joints may have different microstructures and mechanical properties [6,14]. However, few studies have been concerned about the effects of welding layer arrangements on the microstructure and mechanical properties of 5083/6005A dissimilar aluminium alloy joints.

In this work, the microstructure and mechanical properties of 10 mm-thick 5083/6005A aluminium alloy GMAW joints under different welding layer arrangements were investigated. First, the influence of the welding layer arrangement on the microstructure evolution was examined from the perspective of grain boundary liquation, precipitate dissolution and recrystallization. Then, the microhardness and tensile properties were compared. Finally, the thermal cycles under different welding layer arrangements were discussed to analyze the softening behaviour and microstructure evolution. This study will provide experimental data for high-quality and efficient welding of 5083/6005A Al alloys for high-speed trains.

## 2 Experimental

The base metals (BM) were 6005A-T6 and A5083P-O aluminium alloy plates used in the high-speed train, and the filler metal was ER5356 Al−Mg alloy with a diameter of 1.6 mm. The dimensions of the welded plates were 350 mm × 150 mm × 10 mm. The welding machine was a Fronius TransPulse Synergic 5000 welder equipped with an IGM robot welding system. The chemical compositions of the base metals and filler metal are given in Table 1. The tensile strengths of 6005A-T6 Al alloy, A5083P-O Al alloy and ER5356 filler metal are 275, 346 and 361 MPa, respectively.

**Table 1** Chemical compositions of base metals and filler metal (wt.%)

| Material | Mg | Si | Fe | Cu | Mn | Cr | Al |
|---|---|---|---|---|---|---|---|
| 5083 | 4.58 | 0.09 | 0.19 | 0.03 | 0.67 | 0.08 | Bal. |
| 6005A | 0.52 | 0.68 | 0.15 | 0.03 | 0.24 | 0.13 | Bal. |
| ER5356 | 4.9 | 0.04 | 0.12 | 0.02 | 0.14 | 0.012 | Bal. |

As shown in Fig. 1, the plates were assembled and fixed horizontally with a 60° V-shaped groove and a 1 mm assembly gap. A welding backing was used under the aluminium plates to obtain full penetration GMAW joints. The welding direction was parallel to the rolling direction of the base metal. The welding thermal cycle was measured by using a K-type thermocouple with a data acquisition module (NI USB-9211).

In this study, the effects of the welding layer

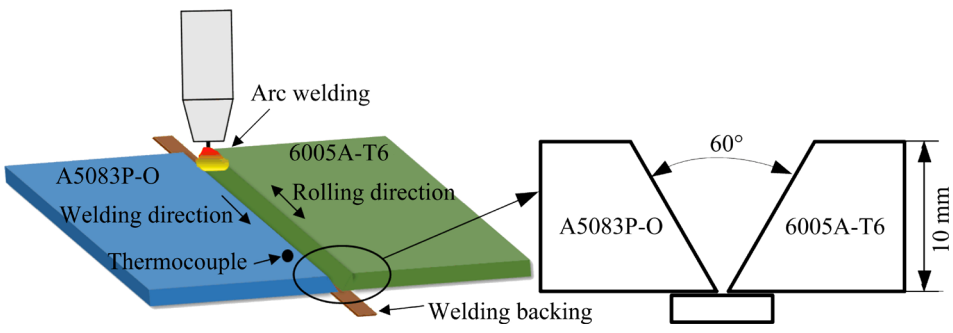


**Fig. 1** Schematic of GMAW of 5083 to 6005A aluminium alloy

arrangement on the microstructure and mechanical properties were investigated by varying the welding layer arrangements, including two layers and two passes, two layers and three passes, and three layers and three passes, as displayed in Fig. 2. For each welding layer arrangement, the processing parameters were optimized in pre-experiments, and the adopted parameters are listed in Table 2.

The microstructure of the joints was examined through an optical microscope (OM, Olympus DSX510), scanning electron microscope (SEM, MERLIN COMPACT) equipped with an electron backscatter diffraction (EBSD) detector, and transmission electron microscope (TEM, JEOL−2100). The EBSD samples were prepared by electropolishing with a solution of 10% perchloric acid and 90% alcohol at a voltage of 20 V for 15 s. The TEM specimens were round foil samples with a diameter of 3 mm and a thickness of 50 μm, prepared by the twin-jet polishing technique. A MICRO-586 microhardness tester was used to test the microhardness distribution of the weld joints with a 100 g load and 10 s dwell time. The tensile test was carried out with a strain rate of 2 mm/min at room temperature on a UTM5105X tester. As shown in Fig. 3(a), a locking bottom structure is formed in the train pillow beam consisting of a 6005A Al profile and 5083 Al plate in actual applications. In the welding process, the role of the locking bottom is similar to that of the welding backing plate. The tensile test of the welding joint was conducted with the backing plate. The geometry of the tensile specimens is shown in Fig. 3(b). After the tensile test, the fracture features of the failed joints were observed by SEM.

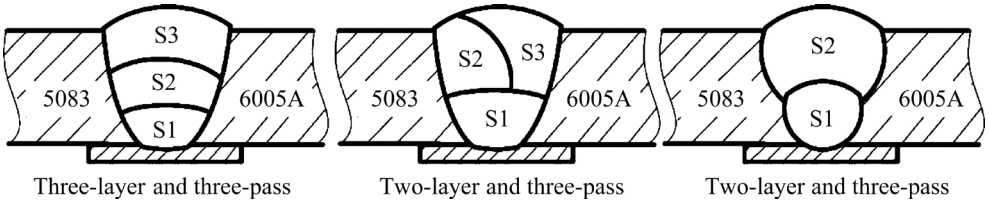


**Fig. 2** Schematic of welding layer and pass arrangement during GMAW of 5083 and 6005A aluminium alloy

**Table 2** Processing parameters employed in this study

| Arrangement | Layer | Current, $I$/A | Voltage, $U$/V | Velocity, $V$/(cm·min$^{-1}$) | Heat input, $E$/(kJ·cm$^{-1}$) |
|---|---|---|---|---|---|
| 2 layers and 2 passes | Bottom layer | 256 | 23.5 | 40 | 9.0 |
| | Top layer | 233 | 23.5 | 43 | 7.6 |
| 2 layers and 3 passes | Bottom layer | 243 | 23.5 | 50 | 6.9 |
| | Top layer 1 | 256 | 23.5 | 52 | 6.9 |
| | Top layer 2 | 245 | 23.5 | 60 | 5.8 |
| 3 layers and 3 passes | Bottom layer | 256 | 23.5 | 60 | 6.0 |
| | Filling layer | 256 | 23.5 | 60 | 6.0 |
| | Top layer | 233 | 23.5 | 60 | 5.5 |

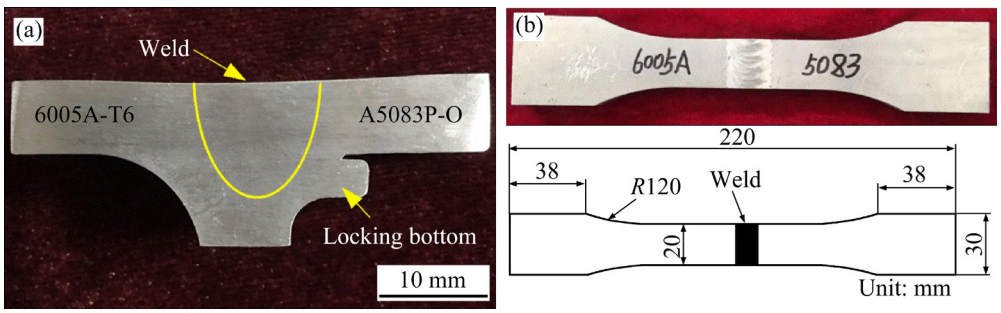


**Fig. 3** Locking bottom structure of joint (a) and geometry of tensile specimen (b)

## 3 Results and discussion

### 3.1 Weld geometry of macrostructure

The weld appearance and cross-section of 5083/6005A GMAW joints are displayed in Fig. 4, and high-quality butt joints were obtained under the three types of welding arrangements. The two-layer and two-pass joints and three-layer and three-pass joints showed a symmetrical weld macrostructure, while the two-layer and three-pass joints showed an asymmetrical weld macrostructure. Moreover, the macroscopic cross-sectional morphology of the two-layer and two-pass joints was V-shaped in Fig. 4(b), while the morphology of the three-layer and three-pass joints was Y-shaped in Fig. 4(f).

### 3.2 Microstructure

The 5083/6005A Al alloy welded joints could be divided into three regions, including the fusion zone (FZ), partially melted zone (PMZ), and heat affected zone (HAZ). The PMZ referred to the narrow region between the FZ and the HAZ and generally experienced thermal cycles where the peak temperature was between the solidus line and liquidus line [15]. As a result, the precipitates ($Mg_xSi_y$) near the grain boundaries dissolved, and a low melting point eutectic (e.g. $\alpha$(A1)+$Mg_2Si$) formed, which was called grain boundary liquation. The microstructure of the PMZ is displayed in Fig. 5. Grain boundary liquation is demonstrated in the PMZ of the two Al alloys. Changing the welding layer arrangements resulted in different microstructures in the PMZ. Severe grain boundary liquation is observed in the two-layer and two-pass joints in Figs. 5(a, d). Moreover, those generated eutectics with low strength led to cracking along grain boundaries on the 6005A Al alloy side under thermal stress, as shown in Fig. 5(d). This was because the heat input of the two-layer and two-pass joints was higher than that of the other two types of welding joints, causing a severer eutectic reaction and thicker liquation film at the grain boundary. During the subsequent cooling stage, the liquation film was subjected to a stronger thermal stress, causing liquation cracking along the grain boundary. In two-layer and three-pass joints, liquation with few cracks was obtained, as shown in Figs. 5(b, e). Note that little liquation is observed in the three-layer and three-pass joints as shown in Figs. 5(c, f), indicating that the grain boundary liquation is closely related to thermal cycles.

In addition, the 6005A Al alloy belongs to the Al−Mg−Si series alloys, and the main liquation mechanism is the eutectic reaction ($\alpha$(A1)+$Mg_2Si$+Si→L, $\alpha$(A1)+$Mg_2Si$→L). The 5083 Al alloy belongs

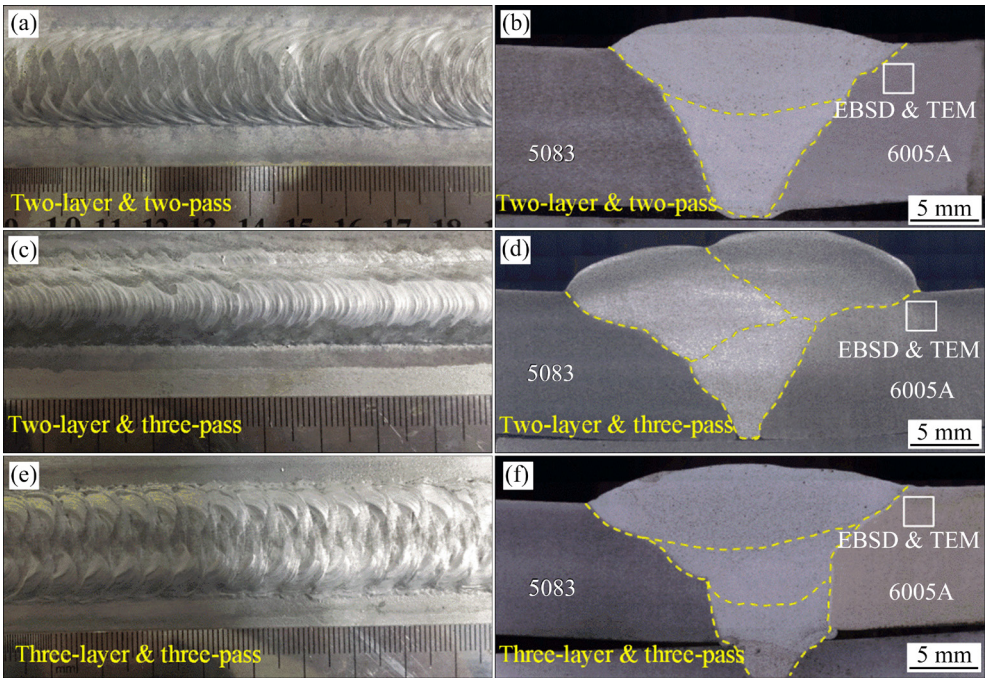


**Fig. 4** Weld appearance (a, c, e) and cross-section (b, d, f) of 5083/6005A Al alloy welded joints: (a, b) Two-layer and two-pass; (c, d) Two-layer and three-pass; (e, f) Three-layer and three-pass

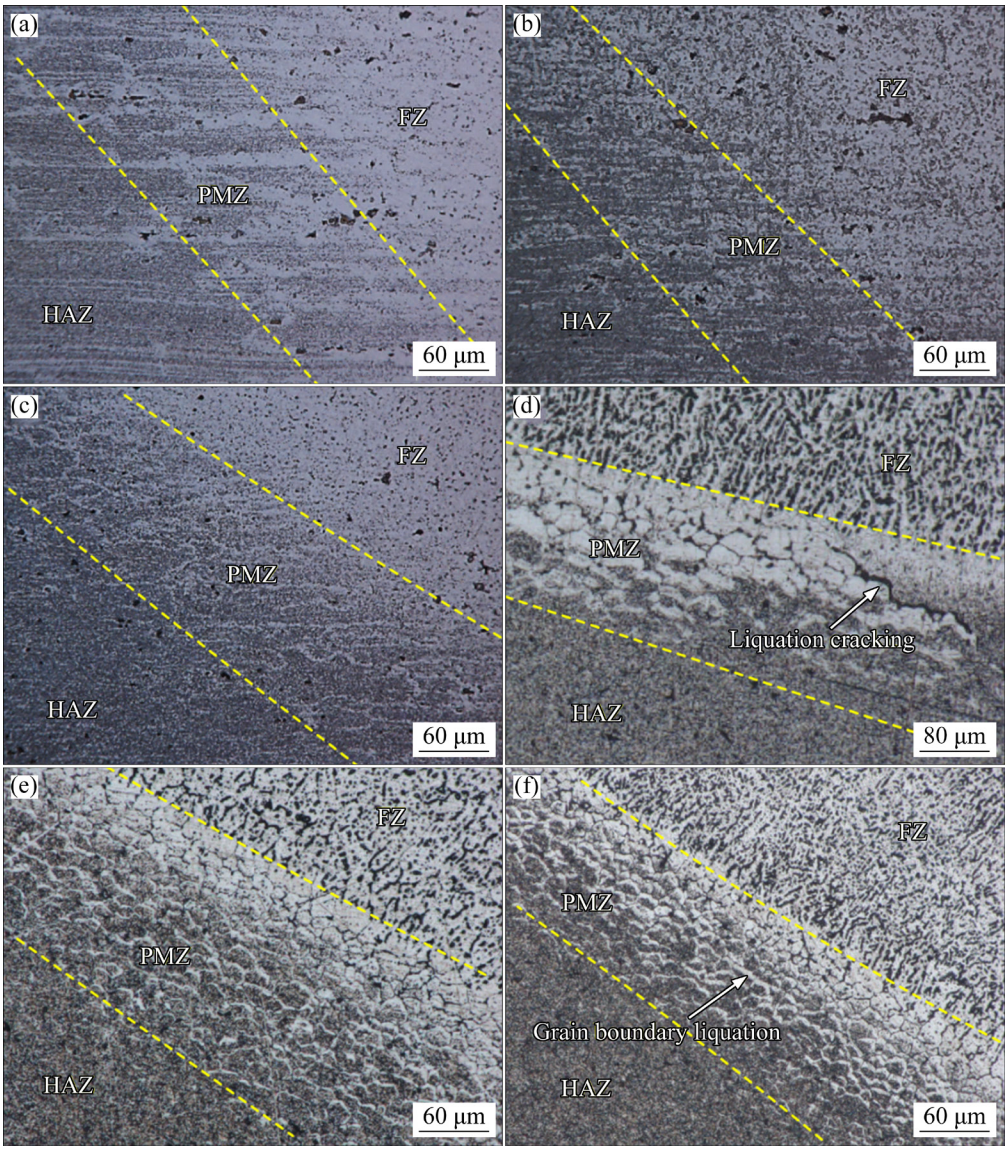


**Fig. 5** Microstructure of PMZ on 5083 Al alloy side (a−c) and on 6005A Al alloy side (d−f): (a, d) Two-layer and two-pass; (b, e) Two-layer and three-pass; (c, f) Three-layer and three-pass

to the Al−Mg series alloys, and the main liquation mechanism is the eutectic reaction ($\alpha$(Al)+$Al_xMg_y \rightarrow$L). Compared with the 5083 Al alloy, the 6005A Al alloy is a ternary alloy and contains a higher content of Si element, which contributes to the wider temperature range of solidification. As liquation cracking is closely related to the temperature range of the coexistence of solid and liquid, the 6005A Al alloy has a higher liquation-cracking sensitivity than the 5083 Al alloy.

According to metallographic analysis, the two layers and two passes welding processes greatly affected the microstructure in the region near the FZ, while the three layers and three passes welding processes caused the least variation. Therefore, the above two joints were selected for further comparison. To study the evolution of the grain structure, EBSD analysis was conducted for the BM and HAZ, and the results are shown in Fig. 6. Cold-rolled grains with obvious crystallographic orientations were verified in the BM, as depicted in Figs. 6(a, d). In the HAZ, the grain size and shape were affected by the welding thermal cycles. On the 5083 Al alloy side, coarse equiaxed grains were obtained, as shown in Figs. 6(b, c). The original cold-rolled grains recrystallized, which was driven by strain and thermal effects. In addition, equiaxed grains that evolved from cold-rolled grains were also observed on the 6005A Al alloy side, as shown in Figs. 6(e, f).

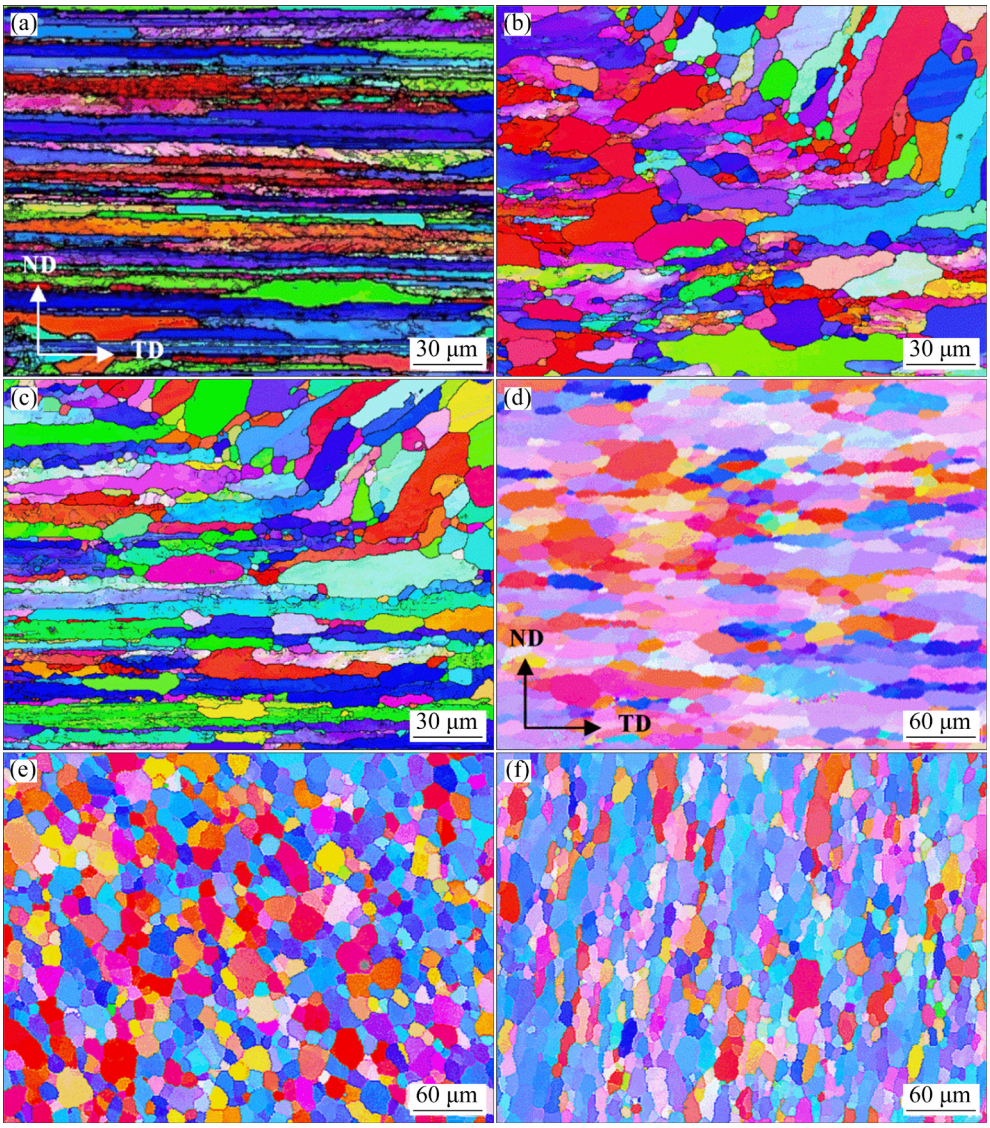


**Fig. 6** Grain structure of welded joints in 5083 alloy (a, b, c) and 6005A alloy (d, e, f): (a, d) BM; (b, e) HAZ in two-layer and two-pass joints; (c, f) HAZ in three-layer and three-pass joints

The statistical results of the grain size are displayed in Fig. 7. Before welding, the grain sizes of the base metal in the 5083 and 6005A Al alloys were 8.56 and 11.48 μm, respectively. In the two-pass and two-layer joints, the average grain size increased to 15.33 μm in the HAZ of 5083 Al alloys and to 12.28 μm in the HAZ of 6005A Al alloys, respectively. However, adopting the three layers and three passes welding processes reduced the grain size to 13.34 and 11.21 μm, respectively. The results indicated that increasing the number of welding layers and passes weakened the extent of recrystallization in the HAZ. Smaller grains benefited the tensile properties. Additionally, a higher level of recrystallization was demonstrated in the HAZ of the 5083 Al alloy. This was because a higher level of the rolling process in 5083 Al sheets caused severer lattice distortion in individual grains as shown in Fig. 6(a), which provided an external driving force for recrystallization.

Considering the great variation in grain structure under different welding arrangements, the precipitates of the welded joints were suggested to be observed because they were thermally sensitive. Transmission electron microscopy (TEM) was used and the results are shown in Fig. 8. Before welding, lath and rod precipitates $Al_x(Mg,Mn)$ were observed in 5083 Al alloy, as depicted in Fig. 8(a). After welding, moderate changes were obtained in the HAZ of the 5083 Al alloy, as shown in Figs. 8(b, c), because $Mg_2Al_3$ was stabler than $Mg_2Si$ and was slightly affected by the thermal

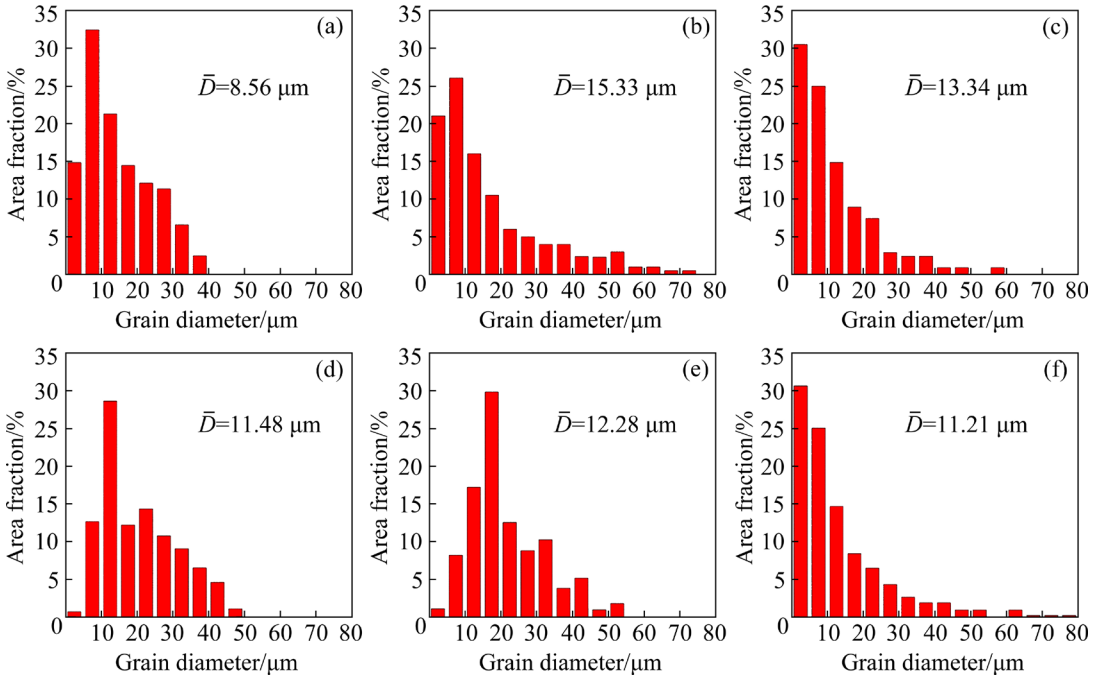


**Fig. 7** Grain size of welded joints in 5083 alloy (a, b, c) and 6005A alloy (d, e, f): (a, d) BM; (b, e) HAZ in two-layer and two-pass joints; (c, f) HAZ in three-layer and three-pass joints

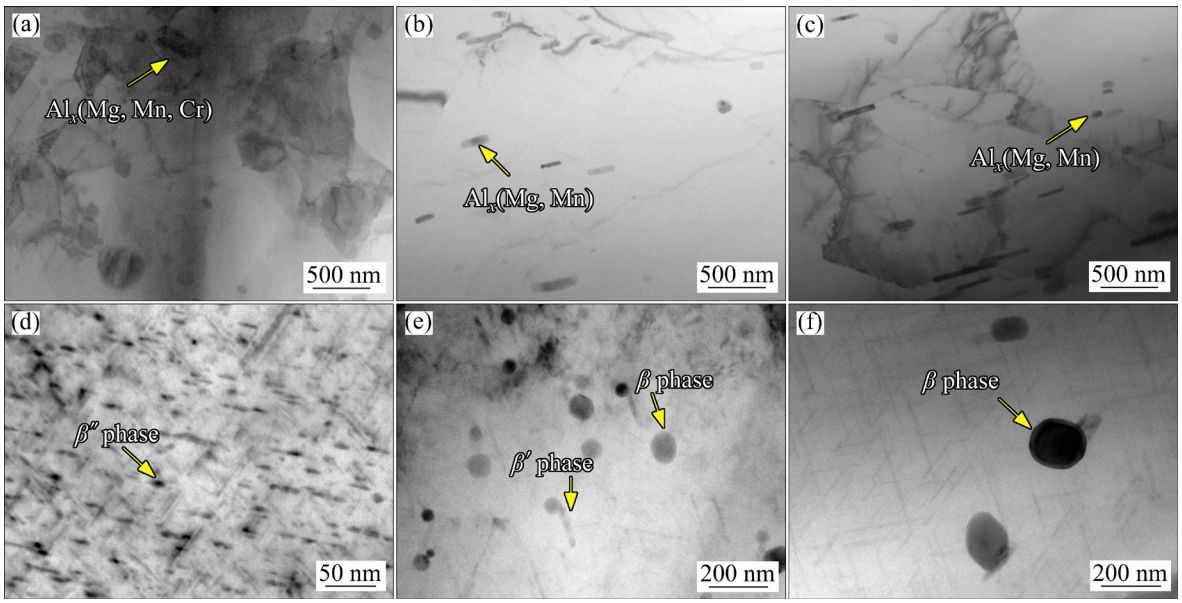


**Fig. 8** Bright-field TEM images of second phase in 5083 alloy (a, b, c) and 6005A alloy (d, e, f): (a, d) BM; (b, e) HAZ in three-layer and three-pass joints; (c, f) HAZ in two-layer and two-pass joints

cycles [16]. However, great changes were observed in the HAZ of 6005A Al alloy. In the base metal of the 6005A Al alloy, thin needle-shaped precipitates $\beta''$ ($Mg_xSi_y$) were examined, as shown in Fig. 8(d), producing strong precipitation strengthening effects. After welding, most $\beta''$ precipitates dissolved in the matrix and transformed into coarse round $\beta$ ($Mg_2Si$) phases in the HAZ of the three-layer and three-pass joints, as shown in Fig. 8(e). This was because the $\beta''$ precipitates were unstable and transformed into the coarse $\beta$ phase [17]. Meanwhile, the quantity of $\beta''$ precipitates further decreased, and the size of $\beta$ phase further increased in the HAZ of two-layer and two-pass joints as shown in Fig. 8(f). The reduction of the strengthening $\beta''$ precipitates significantly influenced the mechanical properties of the welded

joints because precipitation strengthening effects played an important role in enhancing the strength of the 6005A Al alloy.

### 3.3 Thermal cycles

The evolution of the grain structure and precipitates indicated that the welding thermal cycles were not identical when different welding layer arrangements were utilized. To reveal the difference, welding thermal cycles were measured by a K-type thermocouple. To prevent the thermocouple from being melted by arc heat, the thermocouple was inserted in the aluminium plates 10 mm away from the weld toe with a depth of 2 mm, as depicted in Fig. 9(a). As shown in Fig. 9(b), the two-layer and two-pass joints experienced two thermal cycles and the peak temperature reached 370 °C. In the two-layer and three-pass joints, three cycles with a lower peak temperature of 270 °C were obtained. It further declined to 245 °C in the three layer and three passes joints. According to ROBSON and CAMPBELL [18], recrystallization of aluminium alloys generally occurred when the temperature proceeded 300 °C. In addition, the dissolution temperature of $\beta''$ ($Mg_xSi_y$) was lower than 350 °C [19]. The highest temperature in the two-layer and two-pass joints at the test point reached 370 °C. Under this condition, the welding heat input would drive significant recrystallization and precipitate dissolution in the high-temperature region between the test point and fusion line. The decrease in the peak temperature implied a short retention period at high temperatures, resulting in varied degrees of recrystallization and precipitate dissolution. Consequently, the microstructure of the joints was changed differently by adopting different welding layer arrangements.

### 3.4 Microhardness

Figure 10 shows microhardness distribution in the welded joints under different welding layer arrangements. The microhardness of FZ (HV 67−73) slightly fluctuated due to the same filler metal ER5356. However, the microhardness profiles in the HAZ of 5083 and 6005A Al alloys were different.

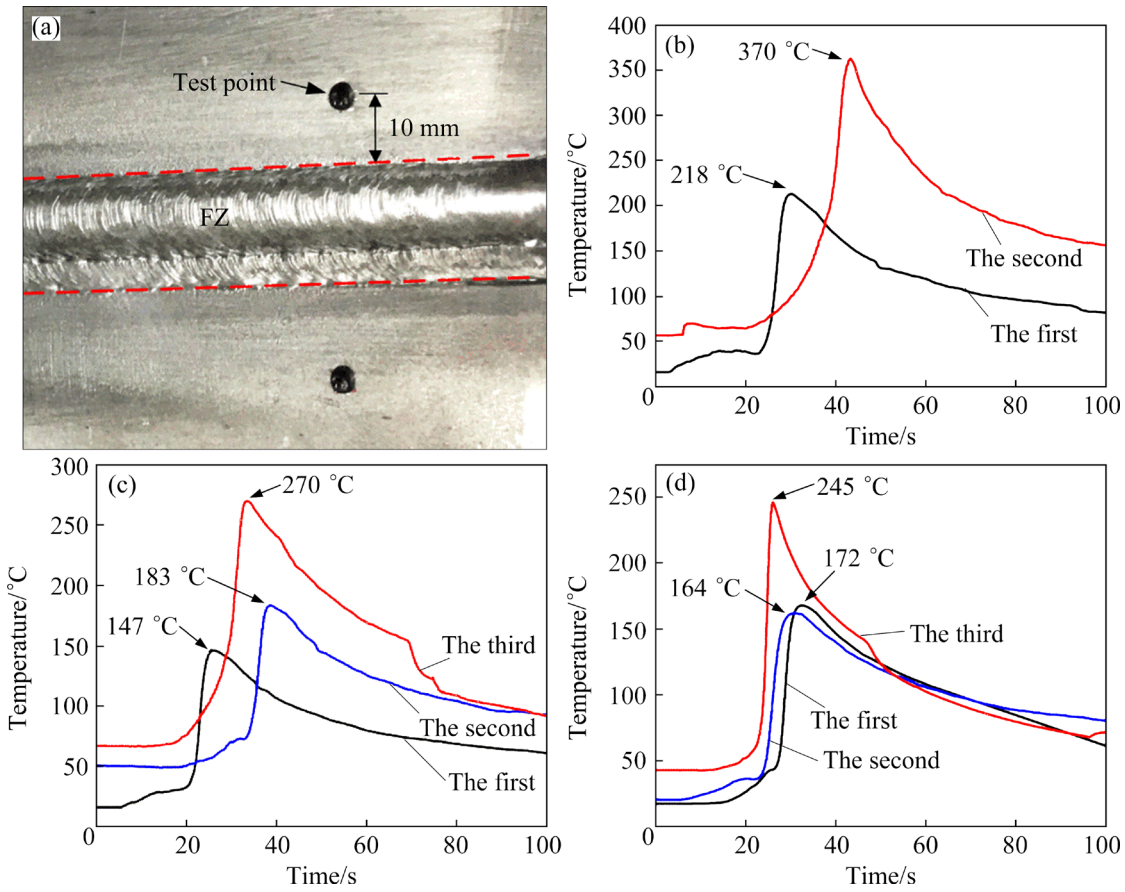


**Fig. 9** Thermal cycles of different welding layer arrangements: (a) Position of thermocouple; (b) Two layers and two passes; (c) Two layers and three passes; (d) Three layers and three passes

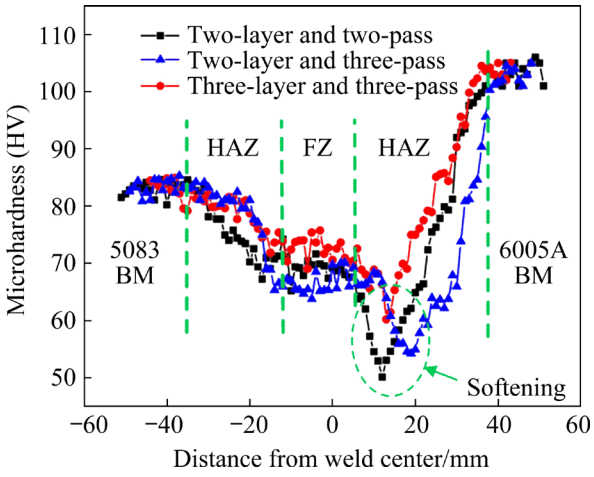


**Fig. 10** Distribution of microhardness in 5083/6005A dissimilar aluminium alloy joints under different welding layer arrangements

On the 6005A Al alloy side, the microhardness of the HAZ sharply decreased to HV 50−60 and then gradually increased to HV 105, implying the formation of a softening zone as depicted in Fig. 10. In the two-layer and two-pass joints, the microhardness of the softening zone was the lowest, only HV 50. However, when applying the three layers and three passes welding processes, the softening was improved, and the lowest microhardness rose up to HV 60. The results indicated that the HAZ in 6005A Al alloys became the weakest region in the joints, while adopting a proper welding layer arrangement could improve the microhardness loss.

On the 5083Al alloy side, the microhardness of the HAZ was only slightly lower than the BM of HV 85, and the main reason for the decrease in microhardness was the change in grain structure caused by recrystallization.

Comparing the hardness profiles of the 6005A and 5083 Al alloys, it could be seen that the softening zone only distributed on the 6005A Al alloy side, but no obvious softening was observed on the 5083 Al alloy side. The difference in softening behaviour was attributed to the different strengthening mechanisms of the 6005A and 5083 Al alloys. The strengthening mechanism of the 6005A Al alloy was precipitation strengthening effects, and the $\beta''$ precipitates were the main strengthening phase. Specifically, the $\beta''$ phase formed at 160−240 °C. However, $\beta''$ precipitates were unstable and transformed to the $\beta'$ or $\beta$ phase when the HAZ rapidly cooled down. Then, the precipitation strengthening effect of $\beta''$ was much better than that of the $\beta$ phase. In multilayer GMAW, multiple thermal cycles further promote the above process. Consequently, the HAZ of the 6005A Al alloy severely softened.

For the 5083 Al alloy, the dislocation at the grain boundary due to lattice distortion by work hardening was the main strengthening mechanism. Under the effects of welding thermal cycles, the loss of mechanical properties due to the change in grain structure by recrystallization was slight, so there was no obvious softening zone in the HAZ of the 5083 Al alloy.

### 3.5 Tensile properties

Figure 11 shows the tensile strength of the 5083/6005A welded joints under different welding layer arrangements. The tensile strength of the two-layer and two-pass joints was 161 MPa. In addition, the tensile strength of the two-layer and three-pass joints reached 178 MPa. When applying three layers and three passes welding processes, the tensile strength of the welded joints further increased to 217 MPa, reaching 79% of the 6005A-T6 Al alloy BM. As shown in Fig. 12, all joints fractured in the HAZ of the 6005A Al alloy, which corresponded with the microhardness profile variation results.

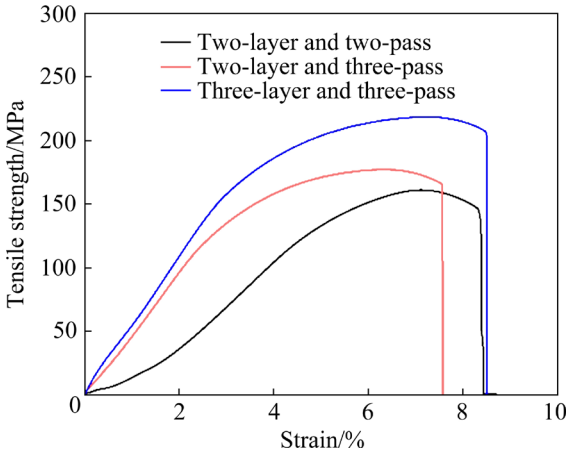


**Fig. 11** Stress−strain curves of 5083/6005A Al alloy welded joints under different welding layer arrangements

The fracture surface of the dissimilar joints was characterized by a number of dimples, as displayed in Fig. 13. Changing the welding layer arrangements promoted different dimple shapes and sizes. Large and shallow dimples appeared on the

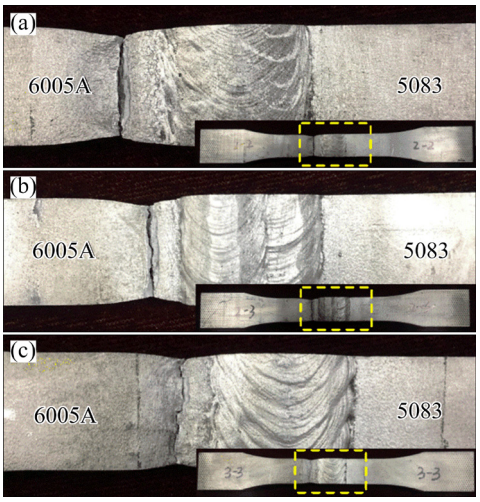


**Fig. 12** Fracture positions of 5083/6005A Al alloy welded joints under different welding layer arrangements: (a) Two-layer and two-pass; (b) Two-layer and three-pass; (c) Three-layer and three-pass

fracture surface of the two-layer and two-pass joints in Figs. 13(a, b), while small, deep and dense dimples were discovered in Figs. 13(c, e). This was attributed to the smaller grain size when more welding layers and passes were adopted. The fracture surface of the three-layer and three-pass joints possessed the most dimples, revealing that their toughness was better than that of the other joints.

The formation of liquation cracking, coarse grains and the decrease in the quantity of precipitates $\beta''$ were believed to be responsible for the failure in the HAZ of the 6005A Al alloy under tensile loading. Although the softening zone could not be avoided and the HAZ of 6005A Al alloy was the weakest part of the joins, optimizing the welding layer arrangements was an effective way to enhance the mechanical properties.

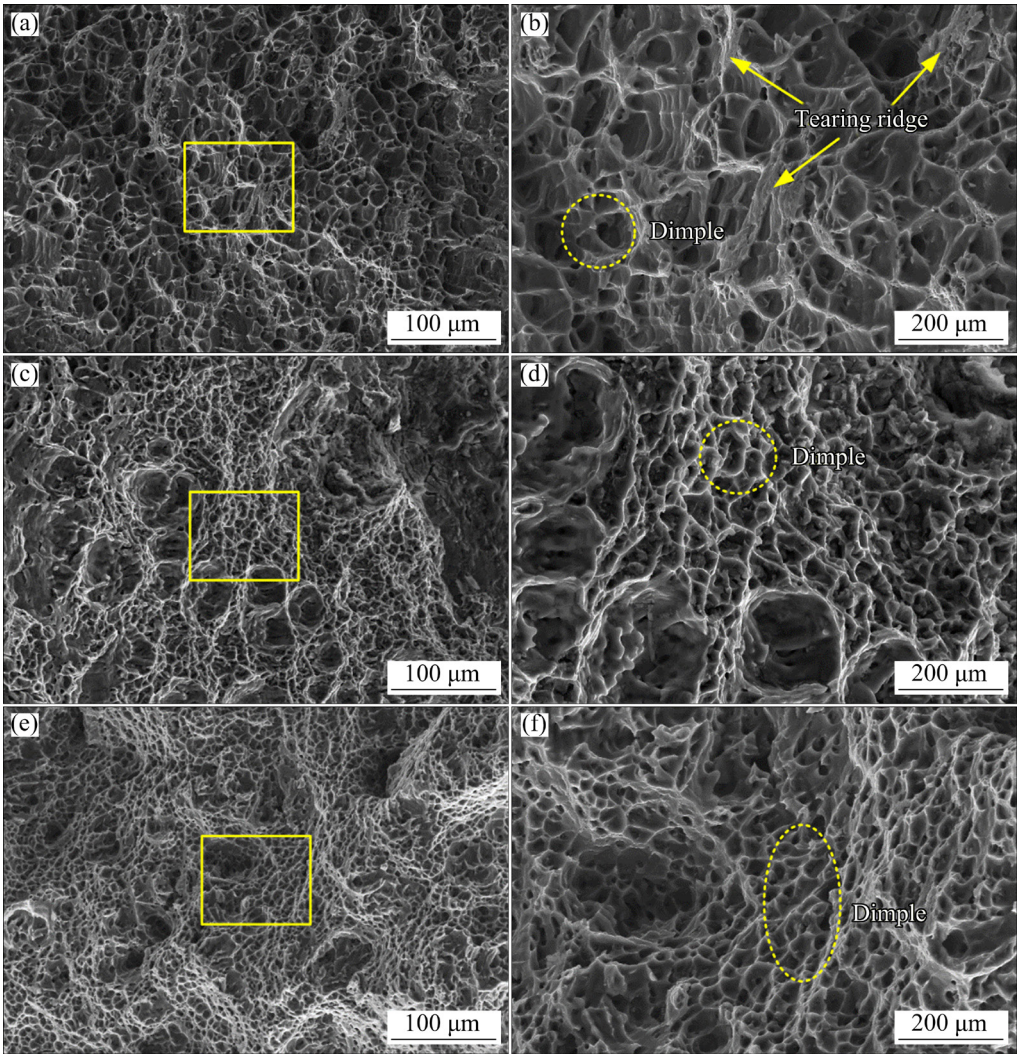


**Fig. 13** Fracture surface of 5083/6005A Al alloy welded joints under different welding layer arrangements: (a, b) Two-layer and two-pass; (c, d) Two-layer and three-pass; (e, f) Three-layer and three-pass

## 4 Conclusions

(1) Welding thermal cycles significantly changed when different welding layer arrangements were adopted. With the increase in the number of welding layer and pass, the peak temperature of the welding thermal cycles gradually decreased. Consequently, the grain boundary liquation, recrystallization and precipitate dissolution were suppressed. The three-layer and three-pass joints possessed the lowest extent of recrystallization and precipitate dissolution.

(2) The precipitates in the HAZ of the 5083 Al alloy were slightly affected by welding thermal cycles. Nevertheless, $\beta''$ precipitates were reduced and coarsened in the HAZ of the 6005A Al alloy. Changing the welding layer arrangement affected the evolution of the precipitates. The fewest precipitates with the largest size were discovered in the two-layer and two-pass joints, leading to severer softening in the HAZ of the 6005A Al alloy.

(3) The three-layer and three-pass joints exhibited a high tensile strength of 217 MPa, reaching 79% of the strength of 6005A Al alloy BM. Although the softening zone could not be avoided, optimizing the welding layer arrangement was an effective way to enhance the mechanical properties.

## Acknowledgments

This work was supported by the National Natural Science Foundation of China (No. 52005132), the Key Research and Development Program of Shandong Province, China (No. 2021ZLGX01), and the Natural Science Foundation of Shandong Province, China (No. ZR2019PEE038). The authors are also grateful to CRRC Qingdao Sifang Co., Ltd., for technical support with aluminum alloy welding experiments and the Heilongjiang Touyan Team for the funding support.

## References

[1] LI Shi-kang, LI Luo-xing, HE Hong, LIU Zhi-wen, ZHANG Long. Influence of dynamic recrystallization on microstructure and mechanical properties of welding zone in Al−Mg−Si aluminum profile during porthole die extrusion [J]. Transactions of Nonferrous Metals Society of China, 2019, 29: 1803−1815.

[2] HUANG Li-jin, WU Dong-sheng, HUA Xue-ming, LIU Shi-chao, JIANG Zhao, LI Fang, WANG Huan, SHI Shao-jian. Effect of the welding direction on the microstructural characterization in fiber laser-GMAW hybrid welding of 5083 aluminum alloy [J]. Journal of Manufacturing Processes, 2018, 31: 514−522.

[3] ZHAO Ying, PEI Jiu-yang, GUO Li-li, YUN Xin-bing, MA Huai-chao. Effects of extrusion speed of continuous extrusion with double billets on welding performance of 6063 Al alloy [J]. Transactions of Nonferrous Metals Society of China, 2021, 31: 1561−1571.

[4] WU Peng-fei, DENG Yun-lai, FAN Shi-tong, JI Hua, ZHANG Xin-ming. A study on dissimilar friction stir welded between the Al−Li−Cu and the Al−Zn−Mg−Cu alloys [J]. Materials, 2018, 11: 1132−1147.

[5] LI Xin-yu, XIA Wei-jun, CHEN Ji-hua, YAN Hong-ge, LI Zhen-zhen, SU Bin, SONG Min. Dynamic recrystallization, texture and mechanical properties of high Mg content Al−Mg alloy deformed by high strain rate rolling [J]. Transactions of Nonferrous Metals Society of China, 2021, 31: 2885−2898.

[6] SHE Xin-wei, JIANG Xian-quan, WANG Pu-quan, TANG Bin-bin, CHEN Kang, LIU Yu-jie, CAO Wei-nan. Relationship between microstructure and mechanical properties of 5083 aluminum alloy thick plate [J]. Transactions of Nonferrous Metals Society of China, 2020, 30: 1780−1789.

[7] HUANG Li-jin, HUA Xue-ming, WU Dong-sheng, JIANG Zhao, YE You-xiong. A study on the metallurgical and mechanical properties of a GMAW-welded Al−Mg alloy with different plate thicknesses [J]. Journal of Manufacturing Processes, 2019, 37: 438−445.

[8] OSTEN J, MILKEREIT B, SCHICK C, KESSLER O. Dissolution and precipitation behaviour during continuous heating of Al−Mg−Si alloys in a wide range of heating rates [J]. Materials, 2015, 8: 2830−2848.

[9] YANG Wen-chao, JI Shou-xun, HUANG Lan-ping, SHENG Xiao-fei, LI Zhou, WANG Ming-pu. Initial precipitation and hardening mechanism during non-isothermal aging in an Al−Mg−Si−Cu 6005A alloy [J]. Materials Characterization, 2014, 94: 170−177.

[10] LIU Hao-bo, YANG Shang-lei, XIE Chao-jie, ZHANG Qi, CAO Ya-ming. Mechanisms of fatigue crack initiation and propagation in 6005A CMT welded joint [J]. Journal of Alloys and Compounds, 2018, 741: 188−196.

[11] LIU Hao-bo, YANG Shang-lei, XIE Chao-jie, ZHANG Qi, CAO Ya-ming. Microstructure characterization and mechanism of fatigue crack initiation near pores for 6005A CMT welded joint [J]. Materials Science and Engineering A, 2017, 707: 22−29.

[12] YAN Zhong-jie, LIU Xue-song, FANG Hong-yuan. Effect of sheet configuration on microstructure and mechanical behaviors of dissimilar Al−Mg−Si/Al−Zn−Mg aluminum alloys friction stir welding joints [J]. Journal of Materials Science & Technology, 2016, 32: 1378−1385.

[13] GUNGOR B, KALUC E, TABAN E, SIK ŞŞ A. Mechanical and microstructural properties of robotic Cold Metal Transfer (CMT) welded 5083-H111 and 6082-T651 aluminum alloys [J]. Materials & Design, 2014, 54: 207−211.

[14] GAO Qing-wei, SHU Feng-yuan, HE Peng, DU Wen-bo. Microstructure and impact mechanical properties of multi-layer and multi-pass TIG welded joints of Al−Zn−Mg alloy plates [J]. Transactions of Nonferrous Metals Society

of China, 2019, 29: 2496−2505.
[15] HUANG C, CAO G, KOU S. Liquation cracking in partial penetration aluminium welds: Assessing tendencies to liquate, crack and backfill [J]. Science and Technology of Welding and Joining, 2004, 9: 149−157.
[16] SVEBSSON L E, KARLSSON L, LARSSON H, KARLSSON B, FAZZINI M, KARLSSON J. Microstructure and mechanical properties of friction stir welded aluminium alloys with special reference to AA 5083 and AA 6082 [J]. Science and Technology of Welding and Joining, 2000, 5: 285−296.
[17] TSAO C S, CHEN C Y, JENG U S, KUO T Y. Precipitation kinetics and transformation of metastable phases in Al−Mg−Si alloys [J]. Acta Materialia, 2006, 54: 4621−4631.
[18] ROBSON J D, CAMPBELL L. Model for grain evolution during friction stir welding of aluminium alloys [J]. Science and Technology of Welding and Joining, 2010, 15: 171−176.
[19] WOO W, CHOO H. Softening behaviour of friction stir welded Al 6061-T6 and Mg AZ31B alloys [J]. Science and Technology of Welding and Joining, 2011, 16: 267−272.

# 焊层排布对 5083/6005A 铝合金熔化极气体保护焊接接头显微组织及力学性能的影响

吴来军[1,2]，韩晓辉[3]，马国龙[3]，杨 彪[1,2]，卞 红[1,2]，宋晓国[1,2]，檀财旺[1,2]

1. 哈尔滨工业大学 先进焊接与连接国家重点实验室，哈尔滨 150001；
2. 哈尔滨工业大学(威海) 山东省特种焊接技术重点实验室，威海 264209；
3. 中车青岛四方机车车辆股份有限公司，青岛 266111

**摘 要**：研究焊层排布方式对 5083/6005A 铝合金熔化极气体保护焊接(GMAW)接头显微组织及力学性能的影响。采用两层两道、两层三道和三层三道 3 种焊层排布方式获得高质量的对接接头。结果表明，位于 6005A 铝合金侧热影响区的软化区是 5083/6005A 铝合金 GMAW 接头的最薄弱部位。两层两道接头的热影响区再结晶程度和沉淀相溶解程度最高，而三层三道接头的最低。随着焊接层数和道次的增加，部分熔化区的晶界液化程度以及软化区的强度损失得到改善。两层两道接头的抗拉强度为 161 MPa，而三层三道接头的抗拉强度提高到 217 MPa。

**关键词**：铝合金；熔化极气体保护焊；焊接层道排布；显微组织；力学性能

**(Edited by Xiang-qun LI)**